Structural and Mechanical Properties of Needle-Punched Nonwoven Reinforced Composites in Erosive Environment

Sachin Tejyan,[1] Amar Patnaik,[1] Amit Rawal,[2] Bhabani K. Satapathy[3]

[1]*Department of Mechanical Engineering, N.I.T., Hamirpur (H.P), India*
[2]*Department of Textile Technology, I.I.T. Delhi, Hauz Khas, New Delhi 110016, India*
[3]*Centre for Polymer Science and Engineering, I.I.T. Delhi, New Delhi 110016, India*

Received 17 February 2011; accepted 4 April 2011
DOI 10.1002/app.34656
Published online 19 August 2011 in Wiley Online Library (wileyonlinelibrary.com).

ABSTRACT: Polypropylene-based needle-punched nonwoven reinforced epoxy composites have been fabricated and were evaluated for their thermomechanical response and dry erosion performance. The erosive wear investigations were carried out using silica sand particles as erodent with varying impact velocity, angles of impingement, fiber content, and stand-off-distance as the operating variables. Design of experiments (DoE) approach-based Taguchi analysis was carried out to establish the interdependence of operating parameters and erosion rate. Impingement angle and impact velocity have been found to be the most significant determinants of erosive wear performance of such nonwoven reinforced composites. The composites were also observed to be appreciably resistant to impact content and indentations in addition to exhibiting the absence of any storage-modulus decay till 60°C accompanied with a nominal increase in the primary transition temperature as revealed from loss-tangent peaks. The composite with 30 wt % and 40 wt % of nonwoven materials have shown the highest and lowest erosion rates, respectively. The morphology of eroded surfaces was examined by using scanning electron microscopy (SEM) and their possible erosion mechanisms are discussed. © 2011 Wiley Periodicals, Inc. J Appl Polym Sci 123: 1698–1707, 2012

Key words: mechanical properties; thermal properties; composites

INTRODUCTION

Needle-punched nonwoven materials primarily consist of fibers in the in-plane direction but some of the fibers are also orientated in the thickness direction. Generally, these nonwovens are produced by repeated penetration of a set of barbed needles on the fibrous web for converting it into coherent and self locking materials.[1] These materials have been explored for numerous industrial and technical applications including abrasive composite materials.[2] Since, nonwoven materials have good blend of strength, lighter in weight, and flexibility in comparison to conventional materials. In addition, these nonwovens have an important quality that provides excellent *z*-directional properties that minimizes delamination problem.

Potentially needle-punched nonwoven composites (NNC) may offer applications in which the materials are subjected to solid particle erosion, such as pipeline carrying sand slurries in petroleum refining, helicopter rotor blades, aircraft operating in desert environments, water turbines, and aircraft engine blades.[3–7] Typically, erosive wear occurs when particle hardness exceeds the material hardness.[8–10] It is widely recognized that polymer and their composites have poor erosion resistance compared with that of metals and some ceramics although the erosion rate of polymer composites invariably remains higher than that of the neat polymers.[11–13] The solid particle erosion behavior of polymer composites as a function of fiber content has been studied to a very limited extent.[14] Tilly and Sage[15] and Rajesh et al.[16] have studied the influence of velocity, impact angle, particle size, and weight of impacted abrasives on nylons, carbon-fiber-reinforced nylon, epoxy resin, polypropylene, and glass-fiber-reinforced plastic. Such independent reports led to the fact that the most influential factors controlling the erosion rate of materials are impact velocity, impact angle of the erodent particles, size, shape, and hardness of erodents.[9]

Despite the promising reports on erosion performance enhancement in polymer composites by fibrous reinforcements, the erosion performance of NNC needs to be thoroughly investigated specifically for their mechano-tribological aspects. In the past, we have reported preliminary results pertaining to fabrication and mechanical characterization of NNC.[7] In this research work, the thermomechanical and erosion wear performance of NNCs have been investigated based on parametric study involving the

Correspondence to: A. Patnaik (amar_mech@sify.com).

parameters namely, erosion rate, impingement angle, and impact velocity.

EXPERIMENTAL DETAILS

Materials and fabrication method

Polypropylene- (PP-) based NNC having constituent nonwoven materials of mass per unit area of 400 g/m^2 along with Epoxy LY 556 (Ciba Geigy India Ltd., Mumbai, India) resin as the binder have been fabricated by hand lay-up technique with different levels of fiber content. The epoxy resin (LY 556) has been cured in the presence of the hardener (HY951) that are mixed in a ratio of 10 : 1 by weight as recommended by the manufacturer. Three composites of different fiber contents, i.e., 20, 30, and 40 wt % were fabricated and the corresponding samples are referred here as NNC20, NNC30, and NNC40, respectively. The castings were subjected to 24 h of postcuring at room temperature. Composites were machined to a dimension of 150 $\times$ 150 mm^2 and cut into required sizes for conforming to standard practices for the evaluation of mechanical properties and solid particle erosion behavior.

Physical and mechanical characterization of NNC

The theoretical density of composite materials in terms of weight fractions can be obtained using the Eq. (1).

$$\rho_{ct} = \frac{1}{(W_f/\rho_f) + (W_m/\rho_m)}, \quad (1)$$

where W and ρ represent the weight fraction and density, respectively. The suffix f, m, and ct correspond to fiber, matrix, and the composite materials, respectively.

The actual density (ρ_{ce}) of the composite, however, can be determined experimentally by simple water immersion technique.[17] The volume fraction of voids (V_v) in the composites is calculated using the following equation:

$$V_v = \frac{\rho_{ct} - \rho_{ce}}{\rho_{ct}}. \quad (2)$$

Microhardness measurement is done using a Leitz microhardness tester. A diamond indenter, in the form of a right pyramid with a square base and an angle 136° between opposite faces, is forced into the material under a load of 10N. The resistance to indentation is measured as the hardness. Low velocity instrumented impact tests are carried out on composite specimens using the Model IT 504 Impact Tester manufactured by TINIUS OLSEN Testing Machine Co. Inc., UK, which calculated and displayed the impact energy absorbed by a specimen. The maximum drop height of 609.6 mm (24 in.) was used in this test and the pendulum has developed the nominal impact velocity of 3.46 m/s in compliance with ASTM and ISO 180 requirements. The standard size of specimen for this test is 80 mm $\times$ 15 mm $\times$ 3 mm. The machine is adjusted such that the blade on the free-hanging pendulum just barely contracts the specimen (zero position). The specimens have been clamped in a square support and are struck at their central point by a rectangular latch catch. Subsequently, the respective values of impact energies of three specimens are recorded directly from the dial indicator.

Dynamic mechanical properties

Dynamic mechanical analysis (DMA) was conducted in a nitrogen atmosphere at a fixed frequency of 1 Hz, heating rate of 5°C/min, a temperature range of 0 to 150°C, and a strain of 1% on rectangular samples with approximate dimensions of 38 $\times$ 12.5 $\times$ 3.5 mm using a Q800 DMA (Crawley, United Kingdom) instrument in bending mode.

Scanning electron microscopy

The eroded composite samples were analyzed using ZEISS EVO Series Scanning Electron Microscope; Model EVO 50 (Oberkochen, Germany) after coating with gold by BIO-RAD POLARAN sputter coater to avoid the electrostatic charging and poor image resolution. To make the sample surface electrically conducting, colloidal silver paste coating on one side (surface to be investigated) of the samples was applied. The worn samples are mounted on stubs to take photomicrographs.

Test apparatus

The solid particle erosion experiments were carried out according to ASTM G76 on the air jet erosion tester TR-471 (Banglore, India) shown schematically in Figure 1. The rig consists of an air compressor, an erodent feeding system, an air particle mixing and accelerating chamber, specimen holder, nozzle, and erodent collector chamber. Dry compressed air is mixed with the particles which are fed at a constant rate from a conveyor-belt type feeder in the mixing chamber and then accelerated by passing through a tungsten carbide nozzle of inner diameter and length of 1.5 mm and 50 mm, respectively. These accelerated particles impact the specimen. The specimen can be held at various angles with respect to the impacting particles using an adjustable sample holder. The feed rate of the particles can be controlled by monitoring the distance between the

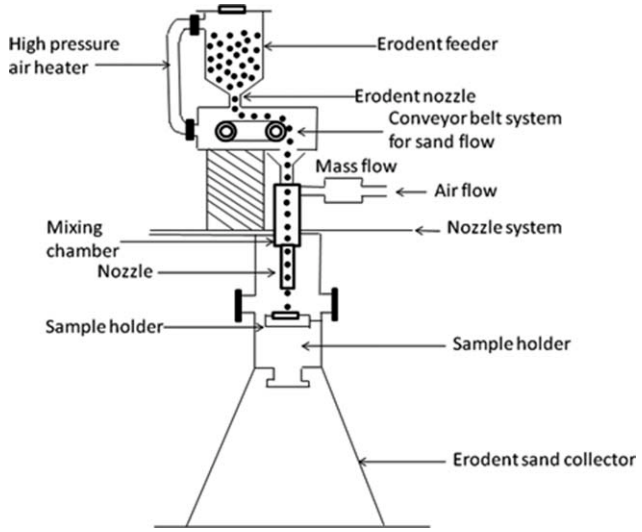

Figure 1 Schematic diagram of an erosion test rig.[7]

particle feeding hopper and the belt drive carrying the particles to the mixing chamber. The impact velocities of the particles can be varied by varying the pressure of the compressed air. The velocity of the eroding particles is determined using a rotating double disc method.[18] In this study, dry silica sand (density: 2.5 g/cm^3) of different particle sizes (250 μm, 350 μm, and 450 μm) is used as erodent. Samples of size 30 mm × 30 mm × (3–5 mm) were cut from the plates for the erosion testes. The samples were cleaned in acetone, dried, and weighed to an accuracy of ±0.1 mg using a precision electronic balance. The specimens are subjected to erosion in the test rig for 15 min and weighed again to determine the weight loss. The ratio of the weight loss to the total mass of the erodent particles that have impacted on the samples is called erosion rate.

Experimental design

The design of experiment (DoE) approach has been adopted for the parametric optimization to reach at a set of operating variables for maximized wear performance. To attain the desired objective, Taguchi analysis has been carried out following L_{27} (3^{13}) orthogonal array design. The details of the selected operating parameters, i.e., impact velocity (A), fiber content in NNC (B), impingement angle (C), stand-off distance (D), and erodent size (E) (each at three levels) under which erosion tests were carried out are given in Table I. In general, the plan of experiments is similar to the design followed earlier[7] and the experimental matrix is shown in Table II. The experimental observations are transformed into single-to-noise (S/N) ratios. The S/N ratio for the minimum erosion rate (maximum erosion resistance) is indicated by a smaller value, which is a better characteristic. This can be calculated as a logarithmic transformation of the mass–loss due to erosion as shown below.

$$\frac{S}{N} = -10 \log \frac{1}{n} (\sum y^2), \tag{3}$$

where "n" is the number of observations, and "y" is the observed data.

RESULTS AND DISCUSSION

Physical and mechanical properties

The density and void content of the composites as shown in Table III have been observed to increase and decrease, respectively, with the increase in the fiber content. The extent of voids remained in the range of 10^{-2} in all the NNCs, indicating better structural integrity of the composites. The mechanical property such as hardness/resistance of the material to indentation has been determined on Rockwell scale [Fig. 2(a)]. It was observed that hardness increased with fiber content, an observation which may be related to low void content and high density of the composites (Table III). The impact energy in an I_{zod} mode has been determined for various composites with different fiber content and is illustrated in Figure 2(b). It was observed that an increase in the nonwoven fiber content has increased its impact energy although the increment may not be significant. This fundamentally implies that impact energy is more limited by the thermosetting epoxy resin than by the ductile NNC.

Dynamic mechanical properties of composites

The dynamic mechanical properties such as storage modulus (E'), loss modulus (E''), and loss tangent (tan δ) (Fig. 3). Figure 3(a) demonstrates the variation of E' against temperature and it is observed that E' remained inappreciably affected in the temperature range of 20–60°C. On further increasing the temperature, the E' suffered a sharp decay specifically in the temperature range of 70–90°C followed by eventual thermomechanical failure of the composites above a temperature of ~ 100°C. Quantitatively,

TABLE I
Levels for Various Control Factors

Control factor	Level I	Level II	Level III	Units
Velocity of impact (A)	35	45	55	m/s
Fiber content (B)	20	30	40	%
Impingement angle (C)	30	60	90	degree
Stand-off distance (D)	65	75	85	mm
Erodent size (E)	250	350	450	μm

TABLE II
Experimental Design Using L_{27} Orthogonal Array

Expt. no.	*A* (m/s)	*B* (%)	*C* (°)	*D* (mm)	*E* (μm)	E_r (g/g)	*S*/*N* ratio (db)
1	35	20	30	65	250	4.7200E-04	66.5211
2	35	20	60	75	350	5.4933E-04	65.2032
3	35	20	90	85	450	5.3333E-05	85.4600
4	35	30	30	75	450	1.5200E-04	76.3631
5	35	30	60	85	250	1.9200E-04	74.3339
6	35	30	90	65	350	3.6000E-04	68.8739
7	35	40	30	85	350	1.0133E-04	79.8849
8	35	40	60	65	450	1.8667E-05	94.5786
9	35	40	90	75	250	1.8133E-04	74.8304
10	45	20	30	75	350	1.3360E-03	57.4838
11	45	20	60	85	450	1.6000E-05	95.9176
12	45	20	90	65	250	9.6000E-04	60.3545
13	45	30	30	85	250	2.3840E-03	52.4538
14	45	30	60	65	350	6.3200E-04	63.9856
15	45	30	90	75	450	1.4933E-04	76.5168
16	45	40	30	65	450	6.1333E-05	84.2460
17	45	40	60	75	250	1.8400E-04	74.7036
18	45	40	90	85	350	5.8667E-05	84.6321
19	55	20	30	85	450	7.8667E-04	62.0841
20	55	20	60	65	250	1.6381E-02	35.7130
21	55	20	90	75	350	2.9680E-03	50.5507
22	55	30	30	65	350	3.8133E-04	68.3739
23	55	30	60	75	450	3.9733E-04	68.0169
24	55	30	90	85	250	3.3067E-04	69.6121
25	55	40	30	75	250	4.0000E-04	67.9588
26	55	40	60	85	350	3.2267E-04	69.8249
27	55	40	90	65	450	6.6667E-05	83.5218

the E' of NNC20 remained at $\sim$ 1900 MPa, whereas that of NNC30 and NNC40 showed a magnitude well above and below at $\sim$ 2000 MPa and $\sim$ 1400 MPa, respectively, in the temperature range of 20–60°C before any modulus decay. However, the mode of E' decay has been found to be very similar in NNC20 and NNC30, whereas the nature of modulus decay in NNC40 has been found to be partially impeded with reference to the effect of temperature, i.e., the E' of composite NNC40 has been observed to be less susceptible to temperature. From Figure 3(b) showing the variation of E'' as a function of temperature, it is apparently observed that the peak temperature corresponding to maximum value of E'' remained unchanged irrespective of the extent of nonwoven fiber content. Theoretically, the temperature corresponding to the maximum value of E'' offers a tentative idea regarding the primary transition temperature of the composite. The peaks corresponding to NNC20 and NNC30 have been observed to be narrower when compared with that of NNC40. A narrow peak, theoretically, indicates that the bulk response of the composite to thermomechanical stresses is more homogeneous in NNC20 and NNC30, whereas the same for NNC40 appeared to be inhomogeneous in terms of its ability to undergo deformation.[19,20] Contrary to the observations from Figure 3(b) showing E'' versus temperature, the primary transition temperatures of the composites, as observed from tan δ values [Fig. 3(c)], have been observed to undergo a nominal shift to higher temperatures with the increase in nonwoven wt %. in the composites. This inevitably indicates that the composites tend to be more damping resistant with the increase in the nonwoven fiber content.

Erosive wear behavior

Taguchi analysis of parametric optimization of erosion performance of NNC

In Table II, the last column represents *S*/*N* ratio of the erosion rate which is the average of two

TABLE III
Theoretical and Experimental Density of Composites

Sl. no.	Fiber content (wt %)	Theoretical density (g/cm^3)	Experimental density (g/cm^3)	Void fraction
1	20	1.0350	1.0078	0.0263
2	30	1.0615	1.0454	0.0152
3	40	1.1245	1.1131	0.0101

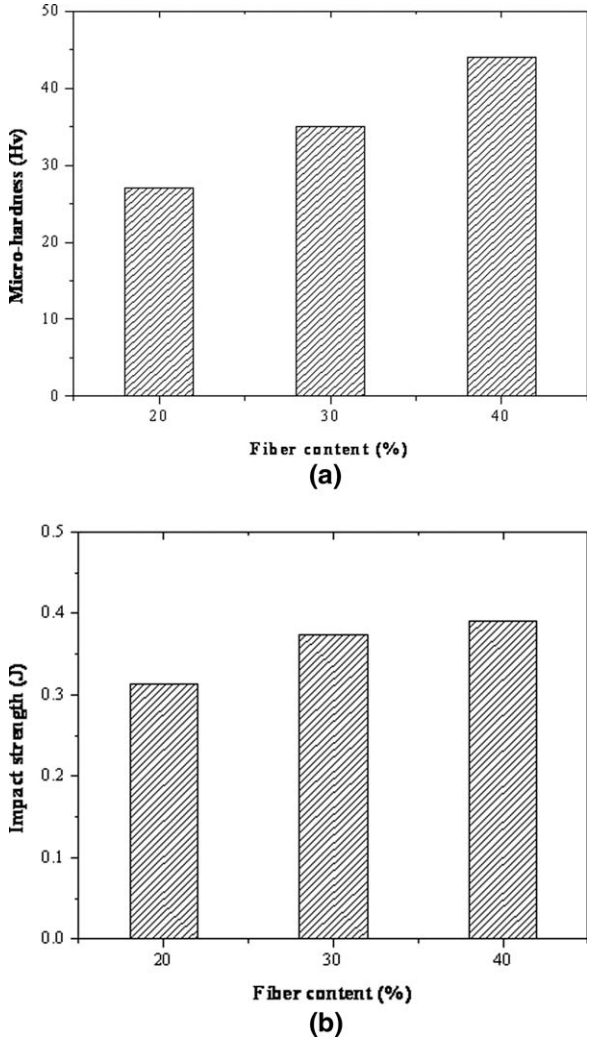

Figure 2 a: Effect of fiber content on Vicker's microhardness of NNC. b: Variation of impact strength with fiber content of the composites.

replications. The overall mean for the S/N ratio of the erosion rate is found to be 70.81 db. The analysis was made using the software MINITAB 14 which is specifically used for design of experiment applications. The factorial design has been taken into account to quantify the interaction effects of the various operating parameters. Analysis of the signal-to-noise (S/N) ratio reveals that factor combination of A_1, B_3, C_3, D_3, and E_1 gives minimum erosion rate (Fig. 4), i.e., maximized erosion resistance. The graphs corresponding to the interactive influences are shown in the Figure 5(a,b).

Anova and the effects of factors

Analysis of variance (ANOVA) was carried out on experimental data to find out the statistical significance of various operating parameters/factors A, B, C, D, and E on erosion rate within confidence level of 5%. Table IV shows the results of the ANOVA with the erosion rate. The last column of the Table indicates that the main effects are highly significant (since they have very small P-values).[21]

From Table IV, it is observed that fiber content ($P = 0.342$), impact velocity ($P = 0.464$), and stand-off

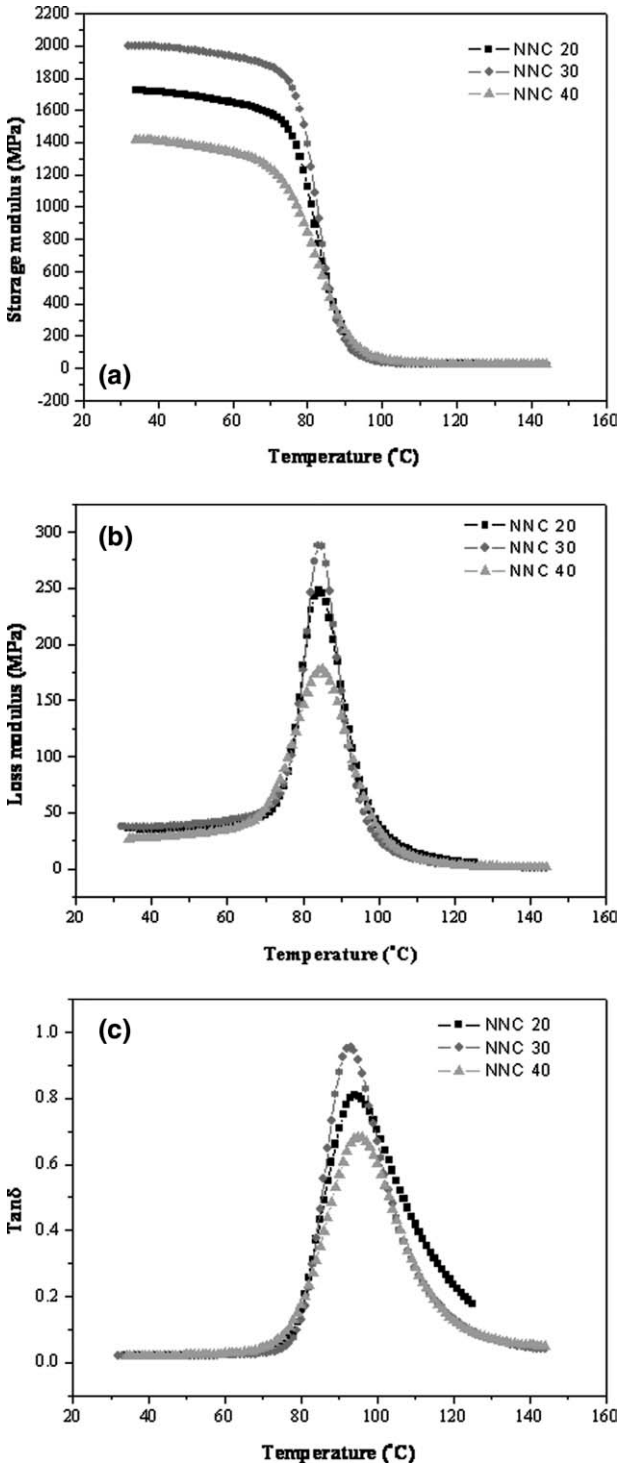

Figure 3 a: Variation of the storage modulus E' as a function of temperature. b: Variation of the loss modulus E'' as a function of temperature. c: Variation of the damping parameter tan δ as a function of temperature.

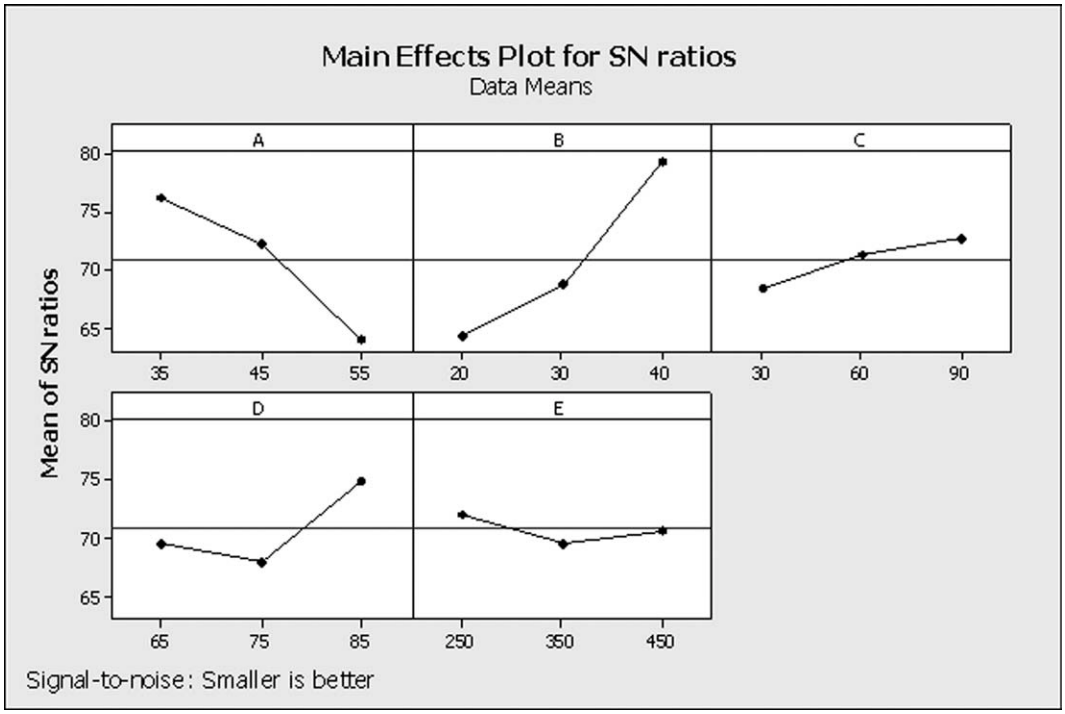

Figure 4 Effect of control factors on erosion rate.

distance ($P = 0.746$) have significant effect on erosion rate. The combined effect of impact velocity and fiber content ($P = 0.819$) shows significant effect on the erosion rate though the remaining other factors and interactions have been observed to be comparatively of lesser significance on erosion rate.

Confirmation experiment

The optimal combination of control factors has already been determined as discussed in the previous section. However, the final step in any design of experiment approach is to predict and verify improvements in the observed values through the use of the optimal combination level of control factors. The confirmation experiment is performed by taking an arbitrary set of factor combination, e.g., $A_3B_2D_2$, whereas factors C and E are omitted (Table IV). However, the factor A though has least effect on performance (erosion resistance), the interactive factor A×B interaction has a significant effect in achieving the performance ideology of minimum erosion rate or maximum erosion resistance as evident from Table IV. Therefore, the factor A is considered in the confirmation experiment while choosing an arbitrary set of factor combination. The estimated S/N ratio for erosion rate may be calculated with the help of following prediction equation:

$$\hat{\eta}_1 = \overline{T} + (\overline{A}_3 - \overline{T}) + (\overline{B}_2 - \overline{T}) + [(\overline{A}_3\overline{B}_2 - \overline{T}) - (\overline{A}_3 - \overline{T}) - (\overline{B}_2 - \overline{T})] + \overline{D}_2 - \overline{T}), \quad (4)$$

where $\overline{\eta}_1$ is the predicted average, $\overline{T}$ is the overall experimental average, $\overline{A}_3$, $\overline{B}_2$, and $\overline{D}_2$ are the mean response of factors and interactions at designated levels.

On simplification, the equation reduces to,

$$\overline{\eta}_1 = \overline{A}_3\overline{B}_2 + \overline{D}_2 - \overline{T}, \quad (5)$$

Thus, the random combination of parameters A_3, B_2, and D_2 lead to S/N of $\overline{\eta}_1$. For each performance, an experiment is conducted for a set of different factor combination and compared with the result obtained from the predictive Eq. (4) as shown in Table V.

The model is capable of predicting erosion rate to a level of reasonable accuracy since the error for the S/N ratio corresponding to the erosion rate remained within 3.79%. However, the error can be further reduced if the number of measurements is increased.

Steady-state erosive wear behavior

Effect of impingement angle and impact velocity on wear characteristic of NNC

The effect of impingement angle on the erosion rate of nonwoven reinforced epoxy composites is shown in Figure 6 while keeping the impact velocity at 35 m/s, stand-off distance at 85 mm, and erodent size at 450 μm. It was observed that the composites showed maximum erosion rate at an impingement

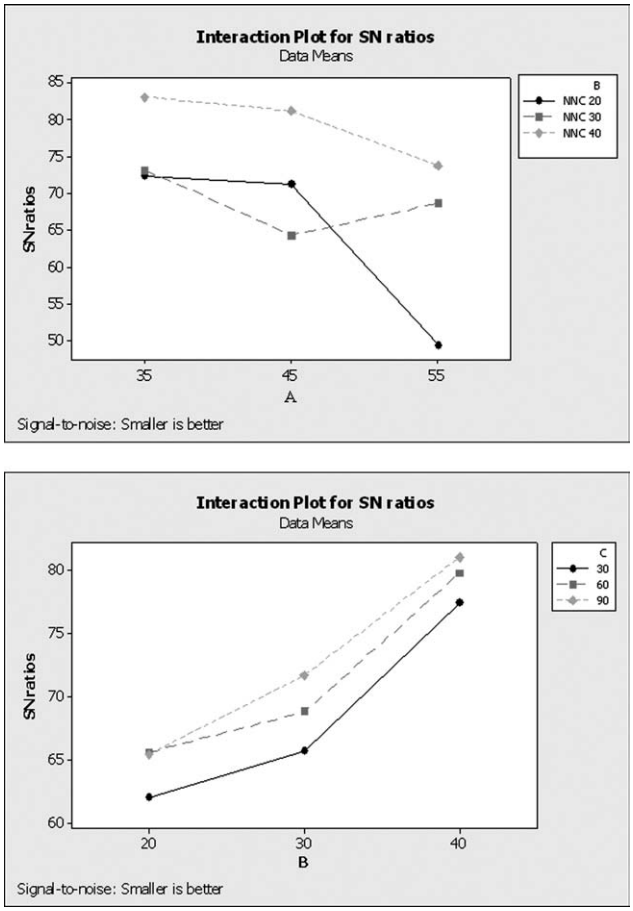

Figure 5 a: Combined effect of factors A and B on erosion rate of NNC interaction graph between (A×B) for erosion rate of NNC. b: Combined effect of factors B and C on erosion rate of NNC interaction graph between (B×C) for erosion rate of NNC.

angle of 45° irrespective of the fiber content. Furthermore, it was observed that the composite NNC40 showed the lowest erosion rate, whereas NNC20 and NNC30 showed higher and moderate erosion rates, respectively. Theoretically, the behavior of ductile materials is characterized by maximum erosion at acute impingement angles, i.e., 15–30°, whereas brittle materials show the maximum erosion at normal impingement angle, i.e., 90°. However, the

TABLE IV
ANOVA Table for Erosion Rate of NNC

Source	DF	Seq SS	Adj SS	Adj MS	*F*	*P*
A	2	705.0	705.0	352.5	0.94	0.464
B	2	1069.8	1069.8	534.9	1.42	0.342
C	2	88.5	88.5	44.2	0.12	0.892
D	2	238.3	238.3	119.2	0.32	0.746
E	2	29.7	29.7	14.8	0.04	0.962
A×B	4	562.0	562.0	140.5	0.37	0.819
B×C	4	9.3	9.3	2.3	0.01	1.000
A×C	4	389.3	389.3	97.3	0.26	0.891
Error	4	1507.3	1507.3	376.8		
Total	26	4599.3				

TABLE V
Results of the Confirmation Experiments for Erosion Rate of NNC

	Optimal control parameters	
	Prediction	Experimental
Level	$A_3B_2D_2$	$A_3B_2D_2$
S/N ratio for erosion rate (db)	65.81	63.32

reinforced composites, unlike the ductile and brittle categories, show a semiductile behavior where the maximum erosion rate is typically reported at an impingement angle of 45–60°.[12] The investigated composites showing maximum erosion rate at an impingement angle of 45° apparently indicate a semiductile mode of erosion. This inevitably has led to the fact that the nonwovens in NNC acts as the determinant in controlling the mode of erosion despite the epoxy based brittle matrix being the binder in these composites. Therefore, the erosion performance in NNC is primarily controlled by the nonwovens which are acting as reinforcement.

Effect of impact velocity on wear characteristic of NNC

The effect of impact velocity on erosion rate of the composites NNC20, NNC30, and NNC40 has been studied by conducting erosion tests at an impact velocity range of 35–55 m/s, whereas the impingement angle, stand-off distance, and erodent size were kept fixed at 60°, 75 mm, and 450 μm, respectively. Figure 7 illustrates the erosion wear rates of the various composites which have shown a higher value of erosion rate at higher impact velocity and thereby demonstrating the congruity of the experimental results

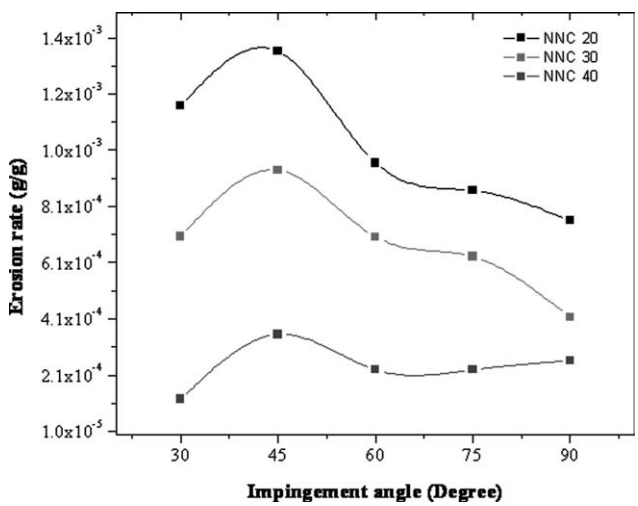

Figure 6 Variation of erosion wear rate with impingement angle.

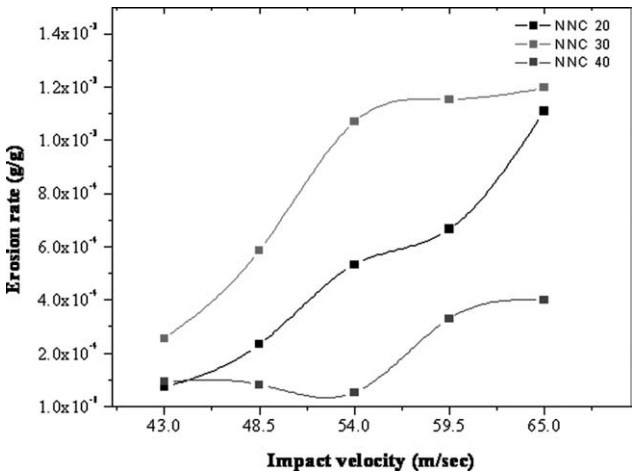

Figure 7 Variation of erosion wear rate with impact velocity.

with the empirically obtained results. Theoretically, erosion rate increases exponentially with the increase in impact velocity and is expressed mathematically as Erosion $= K \times (\text{velocity})^n$, where constant K depends upon impact angle and particle size and n indicates the velocity exponent.[20] Broadly, the magnitude of erosion rates irrespective of the impact angles remained the least in NNC40. It may be mentioned here that the same composite showed the lowest nonrecoverable energy dissipation ability as indicated from E'' data [Fig. 3(b)] and a comparatively higher shift in the primary transition temperature accompanied with a broader tan δ peak [Fig. 4(c)]. Imperatively, such findings indicate that NNC40 resists the thermomechanical stresses induced material deformation till a higher temperature than the composites NNC20 and NNC30.

Wear surface morphology of eroded composites

The eroded surface morphology has been characterized by scanning electron microscopy (SEM) to investigate the systematic influence of factor combinations on the nature of wear and the topographic alterations. For example, the eroded surface micrographs of NNC20 worn under (i) low impact

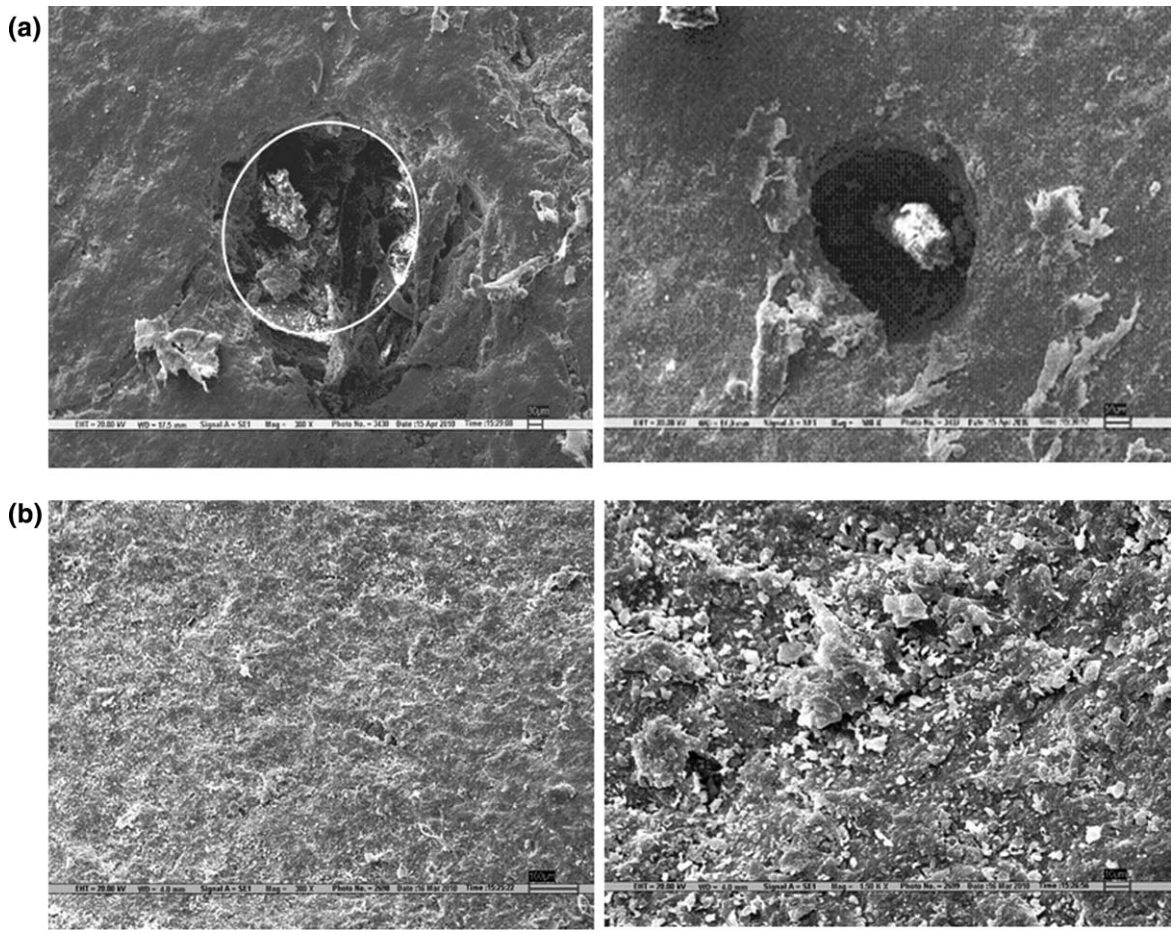

Figure 8 a: SEM micrographs (×300 and ×500) of eroded nonwoven epoxy composite (impact velocity 35 m/s, impact angle 90°, SOD 85 mm, sand particle size 450 μm, and fiber content 20%). b: SEM micrographs (×179 and ×300) of eroded nonwoven epoxy composite (impact velocity 45 m/s, impact angle 60°, SOD 85 mm, sand particle size 450 μm, and fiber content 20%).

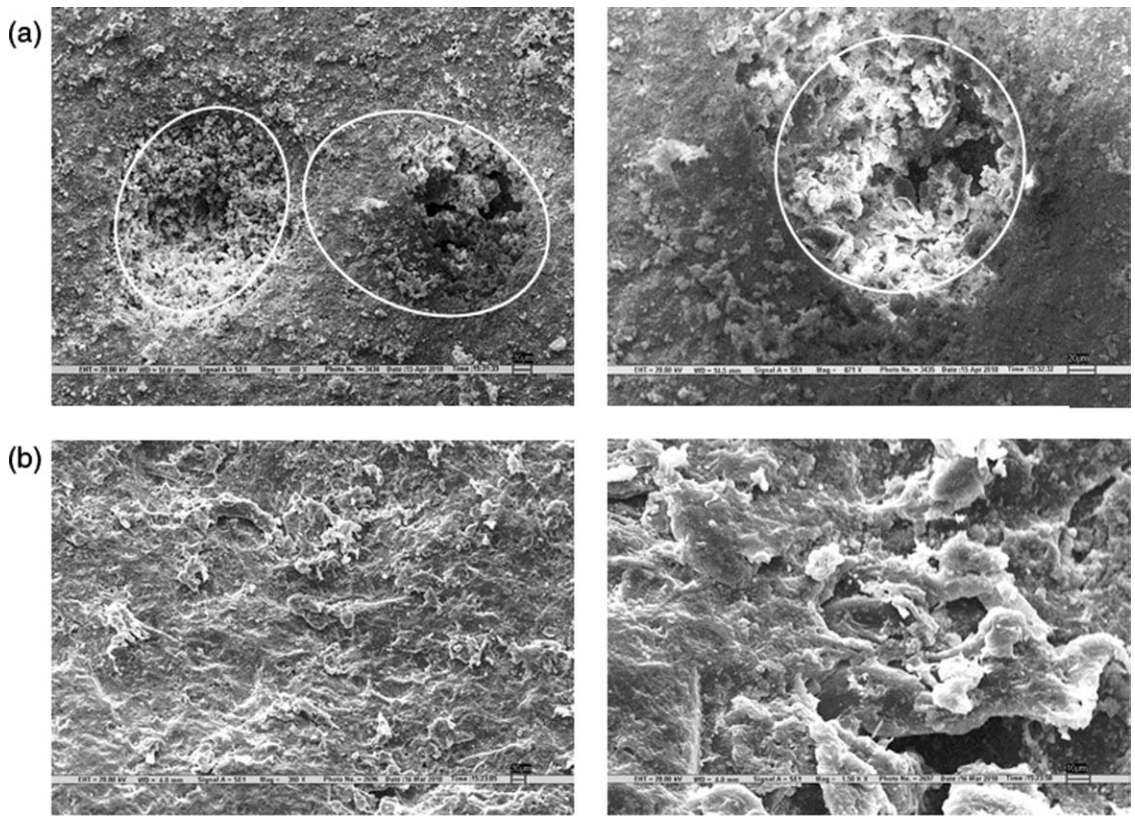

Figure 9 a: SEM micrographs (×400 and ×871) of eroded nonwoven epoxy composite (impact velocity 35 m/s, impact angle 30°, SOD 75 mm, sand particle size 450 μm, and fiber content 30%). b: SEM micrographs (×179 and ×300) of eroded nonwoven epoxy composite (impact velocity 45 m/s, impact angle 60°, SOD 85 mm, sand particle size 350 μm, and fiber loading 30%).

velocity (35 m/s) and high impingement angle (90°) combination and (ii) high impact velocity (45 m/s) and low impingement angle (60°) at a fixed combination of stand-off distance (85 mm) and erodent size (450 μm) are shown in Figure 8. It was observed that at low severity of velocity and impingement angle combination, the material removal takes place via the formation of craters where the displaced material gets deflected into the circumferential periphery of the crater [Fig. 8(a)]. In contrast, at high severity of velocity and impingement angle combination matrix failure has remained the dominating mode of erosion Figure 8(b). This indicates that the composite NNC20 undergoes a brittle failure under high velocity and low impingement angle conditions. The eroded surface micrographs of NNC30 worn under (i) low impact velocity (35 m/s) and low impingement angle (30°) combination and (ii) high impact velocity (45 m/s) and high impingement angle (60°) at a fixed combination of stand-off distance (85 mm) and erodent size (450 μm) are shown in Figure 9. It was observed that under low severity erosion conditions, (i) the composite NNC30 undergoes surface damage resulting in generation of porous craters though the extent of damage remained less intensive [Fig. 9(a)] when investigated under low severity combination of impact velocity (35 m/s) and impingement angle (30°). In contrast, when the composites were eroded under high severity conditions, i.e., under high impact velocity (45 m/s) and high impingement angle (60°) combination, the eroded surface tends to get uniformly damaged showing the generation of severe surface microfracture characteristics without undergoing any substantial plastic deformation [Fig. 9(b)].

CONCLUSIONS

The following salient conclusions have been drawn from the study.

1. Successful fabrication of epoxy-based polymer composites reinforced with needle-punched nonwoven material (PP-400 g/m^2) by simple hand lay-up technique has been achieved.
2. The physical and mechanical properties such as hardness and impact strength increased with the increase in the fiber content in NNC.
3. The thermomechanical attributes have enhanced with the increase in nonwoven fiber mat content. For instance, the broad peak combined with a shift in the primary transition

temperature of the composite and thereby the composite NNC40 exhibits the lowest erosion rate/highest erosion resistance. Thus, NNC40 resists the thermomechanical stresses induced material deformation than the corresponding composites NNC20 and NNC30.

4. Parametric optimization to achieve the maximum erosion resistance for the NNC have been carried out following design of experiment (DoE) approach based on Taguchi analysis. Comprehensively, the parametric combination of impact velocity = 43 m/s, fiber content = 40 wt %, impingement angle = 90°, standoff distance = 85 mm, and erodent size = 450 μm forms the optimum condition for maximization of erosion performance.
5. Impingement angle, impact velocity, and erodent size have been identified as the significant factors (experimental variables) affecting the erosion rate, whereas the fiber content (material variable) plays a crucial role in dramatically altering the erosion rate of NNC.
6. Eroded surface morphology investigations by SEM analysis clearly indicate a change in the mode of crater formation due to impingement/bombardment of erodents as the extent of erosion severity is increased.

References

1. Purdy, A. T. Needle Punching; The Textile Institute: Manchester, 1980.
2. Lukic, S.; Jovanic, P. Mater Lett 2004, 58, 439.
3. Bhushan, B. Principles and Applications of Tribology; Wiley: New York, 1999.
4. Pool, K. V.; Dharan, C. K. H.; Finnie, I. Wear 1986, 107, 1.
5. Kulkarni, S. M.; Kishore, K. Polym Compos 2001, 9, 25.
6. Aglan, H. A.; Chenock, T. A., Jr. SAMPEQ 1993, 41.
7. Patnaik, A.; Tejyan, S.; Rawal, A. Res J Textile Apparel 2010, 14, 12.
8. Friedrich, K. J Mater Sci 1986, 21, 3317.
9. Barkoula, N. M.; Karger-Kocsis, J. J Mater Sci 2002, 37, 3807.
10. Zum Gahr, K. H. Tribol Int 1998, 31, 587.
11. Häger, A.; Friedrich, K.; Dzenis, Y. A.; Paipetis, S. A. In Proceedings of the ICCM-10; Street, K., Whistler, B. C., Eds.; Canada Wood head Publishing Ltd.: Cambridge, 1995; p 155.
12. Barkoula, N. M.; Karger-Kocsis, J. Wear 2002, 252, 80.
13. Tewari, U. S.; Harsha, A. P.; Hager, A. M.; Friedrich, K. Wear 2002, 252, 992.
14. Miyazaki, N.; Takeda, T. J Compos Mater 1993, 27, 21.
15. Tilly, G. P.; Sage, W. Wear 1970, 16, 447.
16. Rajesh, J. J.; Bijwe, J.; Tewari, U. S.; Venkataraman, B. Wear 2001, 249, 702.
17. Agarwal, B. D.; Broutman, L. J. Analysis and Performance of Fiber composites, 2nd ed.; Wiley: New York, 1990.
18. Ruff, A. W.; Ives, L. K. Wear 1975, 35, 195.
19. Ray, D.; Sarkar, B. K.; Das, S.; Rana, A. K. Compos Sci Technol 2002, 62, 911.
20. Yusriah, L.; Mariatti, M.; Abu Bakar, A. J Vinyl and Additive Technol 2010, 16, 98.
21. Montgomery, D. C. Design and Analysis of Experiments, 5th ed.; Wiley: New York, 2005; p 363.